

Relativistic many-body calculations of multipole (E1, M1, E2, M2) transition properties in Al II

Yuan-Fei Wei(魏远飞), Zhi-Ming Tang(唐志明), Xue-Ren Huang(黄学人), Ming-Lu Bu(布明鹭), Xin-Ye Xu(徐信业), and Yi-Yu Cai(蔡翊宇)

Citation: Chin. Phys. B, 2026, 35 (**7**): 073102. DOI: 10.1088/1674-1056/ae0d77
http://cpb.iphy.ac.cn; http://iopscience.iop.org/cpb

What follows is a list of articles you may be interested in

High-precision calculations of highly excited and autoionizing states of the nickel atom

Sheng-Bo Niu(牛生波), Jun-Yao Zhang(张钧尧), Rui Jin(金锐), and Yi-Zhi Qu(屈一至)
Chin. Phys. B, 2026, 35 (**6**): 063101. DOI: 10.1088/1674-1056/ae2a01

High-*Z* benchmarking: Probing the sub-eV frontier and an extensive Li-like uranium atomic dataset

Shuang Li(李双), Yan Wang(王燕), Xue-Lian Chong(崇雪莲), Yan-Ran Luo(罗嫣然), and Fan Zhang(张凡)
Chin. Phys. B, 2026, 35 (**2**): 023103. DOI: 10.1088/1674-1056/ae311a

Theoretical calculations on lifetimes of the low-lying excited states in Lu^{+}

Ting Liang(梁婷), Min Feng(冯敏), Jin Cao(曹进), Yi-Ming Wang(王艺铭), Ben-Quan Lu(卢本全), and Hong Chang(常宏)
Chin. Phys. B, 2025, 34 (**12**): 123101. DOI: 10.1088/1674-1056/ade8e3

Spectroscopy and molecule opacity investigation on excited states of SiS

Rui Li(李瑞), Haonan Lv(吕浩男), Jiqun Sang(桑纪群), Xiaohua Liu(刘晓华), Guiying Liang(梁桂颖), and Yong Wu(吴勇)
Chin. Phys. B, 2024, 33 (**5**): 053101. DOI: 10.1088/1674-1056/ad20dc

Relaxation of Ne^{1+} $1s^{0}2s^{2}2p^{6}np$ produced by resonant excitation of an ultraintense ultrafast x-ray pulse

Jie Yan(闫杰), Yanpeng Liu(刘彦鹏), Yong Hou(侯永), Cheng Gao(高城), Jianhua Wu(吴建华), Jiaolong Zeng(曾交龙), and Jianmin Yuan(袁建民)
Chin. Phys. B, 2023, 32 (**6**): 063101. DOI: 10.1088/1674-1056/acc3fa

---

Relativistic many-body calculations of multipole (E1, M1, E2, M2) transition properties in Al II

Yuan-Fei Wei(魏远飞)[1,2,3], Zhi-Ming Tang(唐志明)[4,†], Xue-Ren Huang(黄学人)[2,3,5,‡], Ming-Lu Bu(布明鹭)[1], Xin-Ye Xu(徐信业)[4], and Yi-Yu Cai(蔡翊宇)[1,6,§]

[1] *Macao Institute of Materials Science and Engineering (MIMSE), Sino-Luso Joint Laboratory for Optoelectronics, Macau University of Science and Technology, Taipa, Macau SAR* 999078, *China*

[2] *Key Laboratory of Atom Frequency Standards, Innovation Academy for Precision Measurement Science and Technology, Chinese Academy of Sciences, Wuhan* 430071, *China*

[3] *University of Chinese Academy of Sciences, Beijing* 100049, *China*

[4] *State Key Laboratory of Precision Spectroscopy, East China Normal University, Shanghai* 200241, *China*

[5] *Wuhan Institute of Quantum Technology, Wuhan* 430206, *China*

[6] *Macau University of Science and Technology, Zhuhai MUST Science and Technology Research Institute, Zhuhai* 519099, *China*

(Received 31 July 2025; revised manuscript received 18 September 2025; accepted manuscript online 30 September 2025)

We present systematic relativistic many-body calculations of multipole transition properties for singly charged aluminum ion (Al II) using a method that combines configuration interaction and many-body perturbation theory (CI + MBPT). Our calculations cover the 103 lowest energy levels in Al II. For five key low-lying states ($3s^2\ ^1S_0$, $3s3p\ ^3P_0$, $3s3p\ ^3P_1$, $3s3p\ ^3P_2$, and $3s3p\ ^1P_1$), we tabulate the transition wavelengths, reduced matrix elements, transition probabilities, and oscillator strengths for about 400 electric dipole (E1), magnetic dipole (M1), electric quadrupole (E2), and magnetic quadrupole (M2) transitions arising from these levels. Our calculated values agree well with available experimental data and other high-precision theoretical calculations, with typical deviations on the order of 1%. Notably, we report over 80% of these transition lines as previously unreported, significantly expanding the existing spectroscopic database for Al II. These results can serve as a valuable reference resource for ongoing precision quantum metrology as well as astrophysical spectroscopy involving the Al II ion.

Keywords: Al II, multipole transition properties, CI + MBPT, relativistic many-body calculations, atomic structure calculation

PACS: 31.15.ag, 31.15.aj, 31.15.am

DOI: 10.1088/1674-1056/ae0d77 **CSTR:** 32038.14.CPB.ae0d77

1. Introduction

The structure of Group IIIA element singly charged ions can be simplified as a tightly bound atomic core with two outer valence electrons. Transitions between states with angular momentum quantum numbers $J = 0$ in these ions are highly insensitive to fluctuations in electromagnetic fields or other environmental perturbations. This property makes these ions, such as Al II, B II, and In II, excellent candidates for optical frequency standards.[1–5] The Al II optical clock, in particular, has achieved exceptional precision with uncertainties at the 10^{-19} level.[6,7] Recently, the Al II optical clock set a new world record again, becoming the most accurate optical clock in the world with an uncertainty of 5.5×10^{-19}.[7] The uncertainties of external-field frequency shifts, caused by fluctuations in electromagnetic fields or an imprecise understanding of atomic structure, represent significant contributions to the uncertainty of the Al II optical clock.[6–12] Accurate theoretical calculations of the atomic spectral properties of Al II, including the energies of states, oscillator strengths of transitions between states, and polarizabilities, are therefore crucial for advancing both atomic theory and the implementation of diverse targeted high-precision experiments, particularly for evaluating external field frequency shifts of the Al II optical clock. Precise theoretical modeling of atomic properties for Al II provides valuable reference data for astrophysical spectroscopy and helps illuminate cosmic evolution processes.[13,14] In addition, accurate transition data are essential for plasma diagnostics, such as electron temperature and density measurements.[15]

Previous theoretical and experimental studies have provided valuable insights into the atomic properties of Al II. On the theoretical front, several computational approaches have been employed, including relativistic configuration interaction Dirac–Fock (CIDF) calculations,[16] multi-configuration Dirac–Hartree–Fock (MCDHF) calculations,[14] multi-configuration Hartree–Fock (MCHF) calculations,[16–18] con-

†Corresponding author. E-mail: zmtang@lps.ecnu.edu.cn
‡Corresponding author. E-mail: hxueren@wipm.ac.cn
§Corresponding author. E-mail: yycai@must.edu.mo

© 2026 Chinese Physical Society and IOP Publishing Ltd. All rights, including for text and data mining, AI training, and similar technologies, are reserved.

figuration interaction plus core polarization method (CICP) calculations,[19] configuration-interaction plus coupled-cluster method (CI + all-order) calculations,[2] relativistic coupled-cluster (RCC) calculations,[20] Fock-space relativistic coupled-cluster (FSRCC) calculations,[21] and finite-field method (FF) calculations.[22] Experimental studies mainly focus on measurements of partial transition properties, such as absolute frequencies and polarizabilities.[1,6,9,12,23]

A simplified energy level structure of Al II is shown in Fig. 1. Early studies established the $3s^2\ {}^1S_0$–$3s3p\ {}^3P_0$ transition in Al II as an optical clock transition with exceptional precision,[1–4,6–12] and recent work has identified the $3s^2\ {}^1S_0$–$3s3p\ {}^3P_2$ transition as a promising candidate for both optical clocks and quantum sensing in searches for new physics.[24] However, prior investigations have predominantly centered on lower-energy states and electric dipole transitions, leaving critical gaps in the systematic characterization of higher-energy states and other transitions — such as the logic transition ($3s^2\ {}^1S_0$–$3s3p\ {}^3P_1$), theoretical cooling transition ($3s^2\ {}^1S_0$–$3s3p\ {}^1P_1$), the new clock transition with potential ($3s^2\ {}^1S_0$–$3s3p\ {}^3P_2$), and other multipole transitions essential for precision experiments.[9] A comprehensive study of multipole transition properties (e.g., wavelengths and amplitudes) is therefore vital to advance both fundamental understanding and applications of Al II.

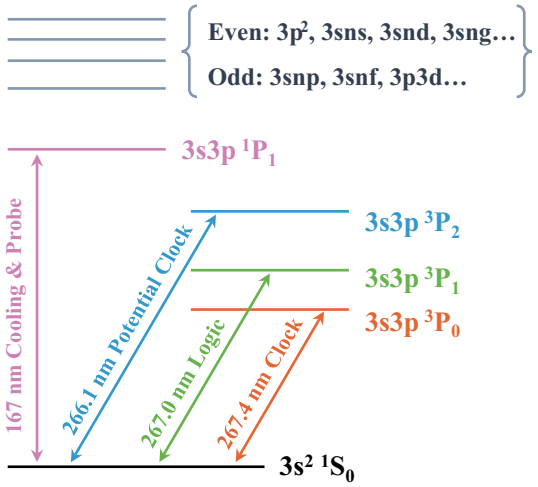


Fig. 1. Simplified energy level structure of Al II.

In this work, we employ configuration interaction and many-body perturbation theory (CI + MBPT) to perform a comprehensive atomic structure analysis of Al II. Our calculations determine the energies of the 103 lowest-lying states, comprising 58 even-parity and 45 odd-parity states. For the five lowest-energy states ($3s^2\ {}^1S_0$, $3s3p^3P_0$, $3s3p^3P_1$, $3s3p^3P_2$, $3s3p^1P_1$), we compute multipole transition properties, including electric dipole (E1), electric quadrupole (E2), magnetic dipole (M1), and magnetic quadrupole (M2) reduced matrix elements, along with their associated transition probabilities and oscillator strengths. These states are particularly relevant for precision measurement applications with Al II, including optical atomic clocks, quantum logic spectroscopy, and quantum state manipulation experiments. For example, accurate calculations of the transition properties of $3s3p^3P_1$–$3s3p^3P_2$ facilitate precise evaluation of the second-order Zeeman shift for new promising clock transitions;[24] accurate calculations of the transition properties of $3s3p^3P_1$–$3s3p^3P_0$ can provide guidance for evaluating external-field shifts in the Al II ion optical clock;[7,9,12] accurate calculations of the energy of $3s3p^1P_1$ are crucial for selecting the appropriate cooling laser wavelength in direct laser cooling experiments of Al II.

The remainder of this paper is organized as follows. Section 2 presents the theoretical framework, including general formulas for radiative transition properties and an overview of the CI + MBPT method as applied to two-electron systems. In Section 3, we compare our numerical results with available theoretical and experimental data, including reference values from the National Institute of Standards and Technology (NIST) atomic spectra database.[25] Section 4 concludes with a summary of our findings. All transition data, including the transition wavelengths, reduced matrix elements, transition probabilities, and oscillator strengths, for the approximately 400 multipole lines are compiled in Tables S1–S6, provided in the supplementary material.

2. Method of calculations

2.1. CI + MBPT method

The CI + MBPT method is employed for calculating atomic structures within the framework of relativity, which fully combines the advantages of the configuration interaction (CI) method and many-body perturbation theory (MBPT) method.[26,27] The CI method considers the correlation effect between valence electrons (VV) under the approximation of a "frozen" core, while the MBPT method captures both the correlation effect between core electrons and that between core and valence electrons.[26,27] The effectiveness of CI + MBPT has been extensively validated, with many studies demonstrating excellent agreement between calculated results and high-precision experimental measurements.[26–34]

The wave function of the valence electronic states in the CI method, $\Psi(\gamma PJ)$, consists of a linear combination of a set of configuration wave functions with specific angular momentum J and parity P. It can be expressed as follows:[26,27]

$$\Psi(\gamma PJ) = \sum_{i=1}^{M} c_i \Phi(\gamma_i PJ), \tag{1}$$

where $\Phi(\gamma_i PJ)$ represents a configuration wave function in an M-dimensional CI model space, c_i denotes the linear combination coefficient, and γ_i represents the unspecified remaining quantum number. The CI model space encompasses wave

functions constructed from single (S) and double (D) excitations of valence electrons from the selected reference group to certain virtual orbitals. The configuration wave function is defined by the Slater determinant constructed from single-electron Dirac orbitals. The single-electron Dirac orbital can be expressed as[26,27]

$$\phi_{nkm}(r,\theta,\varphi) = \frac{1}{r}\cdot\frac{P_{nk}(r)\cdot\Omega_{km}(\theta,\varphi)}{\mathrm{i}Q_{nk}(r)\cdot\Omega_{-km}(\theta,\varphi)}, \tag{2}$$

where $P_{nk}(r)$ and $Q_{nk}(r)$ are the radial wave functions, $\Omega_{km}(\theta,\varphi)$ represents the angular wave function, n is the principal quantum number, $k=\pm(j+1/2)$ is the relativistic quantum number, and m is the magnetic quantum number corresponding to the total angular momentum of a single electron. In this work, the reference configurations for the even-parity states of Al II are $3s^2$, 3s4s, and 3s3d, the reference configuration for the odd-parity states is 3s3p, and the maximum orbitals of the single and double excitations are 29s, 29p, 29d, and 29f. The single-electron orbitals include 1s–29s, 2p–29p, 3d–29d, and 4f–29f, where the real orbitals ($n<2$) and 3s, 4s, 3p, 4p, 3d, 4d, and 4f orbitals are obtained by solving the Dirac–Hartree–Fock (DHF) equation under the V^{N-2} approximation, and the remaining virtual orbitals are automatically generated by the recursive program.[27] For the selection of the number of electron correlations, specifically the choice of the maximum excited orbitals, we conducted a rigorous convergence test. We compared the energy values of different maximum excited orbitals, calculated for at least five energy levels, with the results from the NIST database, as shown in Fig. 2. The horizontal axis represents the principal quantum number of the maximum excited orbitals, while the vertical axis shows the ratio relative to the NIST results. The electron correlation effects exhibit progressive attenuation with increasing principal quantum number, and this diminishing influence reaches convergence at $n=29$; the differences between the selected energy values and those from the NIST database converge to within 0.2%. Orbitals with $n>29$ demonstrate negligible contributions to the overall correlation energy, establishing this quantum number as the practical cutoff threshold for our computational framework. In the trial calculation process, we performed a strict convergence test on the radial integration range ($R_{\max}$ parameter), and finally selected the radial integration range as $R_{\max}=250$ a.u.

The wave function of the valence electron state n is determined by solving the energy eigenvalue equation. The energy eigenvalue equation is expressed as[26,27]

$$H\Psi_n = E_n\Psi_n. \tag{3}$$

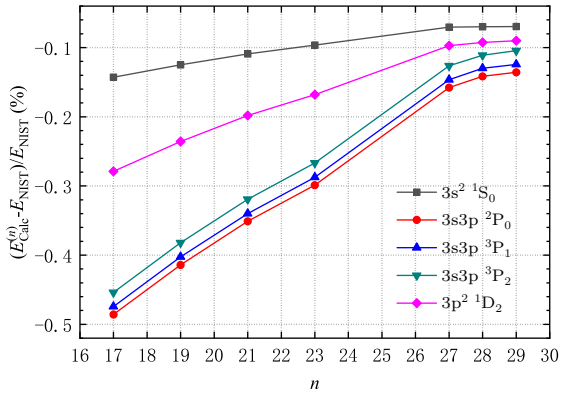


Fig. 2. Convergence test of the energy values of the five lowest-energy levels.

The CI Hamiltonian of valence electrons takes the form[26–34]

$$H_{\rm CI} = \sum_{i=1}^{2}\left[c\boldsymbol{\alpha}_i\cdot\boldsymbol{p}_i+(\beta_i-1)c^2+V_{\rm nuc}(r_i)+V^{N-2}(r_i)\right] + \frac{1}{2}\sum_{i,j=1}^{2}V_{\rm c}(r_{i,j})+H_{\rm core}, \tag{4}$$

where c denotes the speed of light in a vacuum, $\boldsymbol{\alpha}$ and β are Dirac matrices, $\boldsymbol{p}$ represents the momentum operator, $V_{\rm nuc}(r)$ is the nuclear potential, $V^{N-2}(r)$ describes the DHF potential from the core electrons, and $V_{\rm c}(r_{1,2})$ denotes the inter-electron Coulomb potential at a distance $r_{1,2}$. $H_{\rm core}$ denotes the energy of the frozen core, which usually cancels out in the evaluation of excitation energies or transition matrix elements. The Breit interaction (specifically, the Gaunt term as the dominant contribution) can be included in the CI Hamiltonian (Eq. (4)) through complete diagonalization.[27] The CI+MBPT method extends this framework by incorporating all valence-core (VC) and core-core (CC) correlations into the effective Hamiltonian $H_{\rm eff}$ through the many-body perturbation theory method. The effective Hamiltonian $H_{\rm eff}$ can be expressed as follows:[26,27]

$$H_{\rm eff} = H_{\rm CI}+\Sigma_1(r_1)+\Sigma_1(r_2)+\Sigma_2(r_1,r_2), \tag{5}$$

where Σ_1 represents the single-electron correlation operator, describing the correlations between a single valence electron and the core; Σ_2 denotes the two-electron correlation operator, which describes the screened Coulomb interaction between valence electrons mediated by the core. More specific forms of these correlation operators can be found in Refs. [26,27]. These correlation operators, treated to second order in MBPT, capture all valence-core and core-core correlations in the effective Hamiltonian. Solving the energy eigenvalue equation with $H_{\rm eff}$ thus accounts for electron correlations throughout the atomic system. In our calculation, all valence-valence correlations are included directly in the matrix diagonalization, and the energy-dependent expressions for the operators Σ_1 and Σ_2 correspond to Brillouin–Wigner perturbation theory.[26] The

CI + MBPT package used in this work was developed by Kozlov *et al.*, and the specific program operation process can be referred to Ref. [27]. Quantum electrodynamic effects (self-energy and vacuum polarization) are not included in this study, as their contributions are expected to be very small compared with the current level of theoretical accuracy.

2.2. Transition probabilities and oscillator strengths

We present general expressions for multipole transition properties in atomic systems, including transition rates, oscillator strengths, and line strengths. For transitions between an upper state i and a lower state k, the transition rates (in s^{-1}) for electric dipole (E1), electric quadrupole (E2), magnetic dipole (M1), and magnetic quadrupole (M2) transitions take the following forms:[28,35,36]

$$A_{ki}^{E1} = \frac{2.02613\times10^{18}}{\lambda^3}\cdot\frac{S_{ik}^{E1}}{2J_i+1}\,s^{-1}, \tag{6}$$

$$A_{ki}^{E2} = \frac{1.1199\times10^{18}}{\lambda^5}\cdot\frac{S_{ik}^{E2}}{2J_i+1}\,s^{-1}, \tag{7}$$

$$A_{ki}^{M1} = \frac{2.69735\times10^{13}}{\lambda^3}\cdot\frac{S_{ik}^{M1}}{2J_i+1}\,s^{-1}, \tag{8}$$

$$A_{ki}^{M2} = \frac{1.49097\times10^{13}}{\lambda^5}\cdot\frac{S_{ik}^{M2}}{2J_i+1}\,s^{-1}. \tag{9}$$

The dimensionless oscillator strengths f_{ik} are related to the transition rates A_{ki} through $f_{ik} = 1.4992\times10^{-16}\times\frac{2J_k+1}{2J_i+1}A_{ki}\lambda^2$. The corresponding E1, E2, M1, and M2 oscillator strengths can be derived as follows:[35,36]

$$f_{ik}^{E1} = \frac{303.756}{\lambda(2J_k+1)}S_{ik}^{E1}, \tag{10}$$

$$f_{ik}^{E2} = \frac{167.90}{\lambda^3(2J_k+1)}S_{ik}^{E2}, \tag{11}$$

$$f_{ik}^{M1} = \frac{0.00404386}{\lambda(2J_k+1)}S_{ik}^{M1}, \tag{12}$$

$$f_{ik}^{M2} = \frac{0.00223526}{\lambda^3(2J_k+1)}S_{ik}^{M2}. \tag{13}$$

The numerical factors above incorporate unit conversions and fundamental constants.[28,35,36] In these equations, λ is the wavelength in vacuum of the transition measured in angstroms (Å), $S_{ik}^{O} = |\langle i\|O\|k\rangle|^2$ represents the line strength corresponding to the transition type, and $\langle i\|O\|k\rangle$ represents the reduced transition matrix element (RME) for the corresponding transition.

3. Results and discussion

3.1. Energies

We present the energies of the ground state and 102 lowest excitation states (57 even-parity states and 45 odd-parity states) of Al II calculated using both the pure CI method and the CI + MBPT method. Results for even- and odd-parity states, along with the effects of the Breit interaction, are presented in Tables S1 and S2, respectively, of the supplementary material. We have previously applied these methods to study the dynamic E1 polarizabilities of Al II, and a small number of energy values have already been published.[32] We compare our results with available experimental measurements, previous theoretical calculations,[2,14,16,18–22,24,36–39] and reference values from the NIST atomic spectra database.[25] Specifically, our calculated results agree best with those of Papoulia *et al.*,[14] with most differences being less than 1%. However, deviations between our results and the NIST atomic spectra database values are reduced by about 50% compared with those reported in Ref. [14]. For the fine-structure splitting, the ordering of the split energy levels from our calculations exhibits better agreement with the NIST database data compared with those reported in Ref. [14].

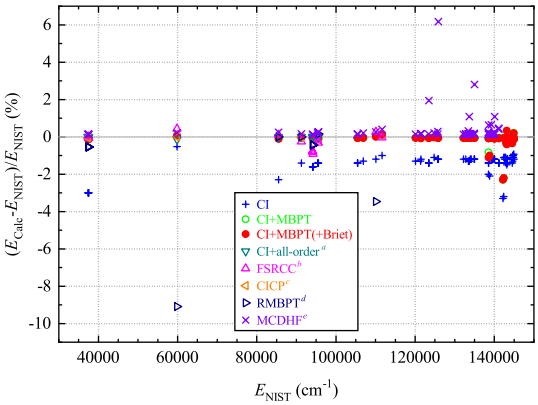


Fig. 3. Comparison of energy level calculations obtained using different methods. The horizontal axis shows NIST database values (in cm^{-1}), and the vertical axis shows the relative differences between the calculated values (from CI + MBPT and other theoretical methods) and the NIST reference data (in percentage). References: [a]Safronova *et al.* (2011);[2] [b]Kumar *et al.* (2021); [21] [c]Mitroy *et al.* (2009);[19] [d]Johnson *et al.* (1997);[37] [e]Papoulia *et al.*[14]

Figure 3 compares our CI + MBPT calculated energies with NIST reference values, showing the relative differences as a function of state energy. Our CI + MBPT results demonstrate excellent agreement with both experimental measurements and previous theoretical calculations, with differences typically below 3%. Compared with NIST reference values, our calculations show deviations of less than 0.2% for most states, with absolute differences generally below 100 a.u. Larger deviations, exceeding 1% in four cases, occur primarily for states with high principal quantum numbers, which are known to present computational challenges due to their complex configuration structures.[2,9,16,18–22,25,36,37] Following the evaluation criteria for transition probability accuracy from the NIST atomic spectra database, we also compare our calculated energies with the experimental and theoretical results in the NIST atomic spectra database to assess and classify the accuracy of our data. Based on the relative differences from

the experimentally recommended values of the NIST spectral database, we define the classification criteria for accuracy as: $AA \leq 0.03\%$, $A+ \leq 0.07\%$, $A \leq 0.1\%$, $B+ \leq 0.7\%$, $B \leq 1\%$, $C+ \leq 10\%$, $C \leq 20\%$, $D+ \leq 40\%$, $D \leq 50\%$, and $E > 50\%$. The accuracy distribution of the calculated energy values is shown in Fig. 4.

The incorporation of many-body perturbation theory significantly improves the accuracy of our results, showing improvements of 1–2 orders of magnitude compared with pure CI calculations. The Breit interaction contributions are found to be small, with relative effects below 0.01%, indicating that the valence electron correlation model effectively describes the atomic structure of Al II. Our calculations successfully capture both valence and core electron correlations, producing accurate results even for challenging high-lying states. This systematic set of energy level calculations, including states with high principal quantum numbers and orbital angular momenta, provides valuable reference data for future experimental spectroscopic studies of Al II.

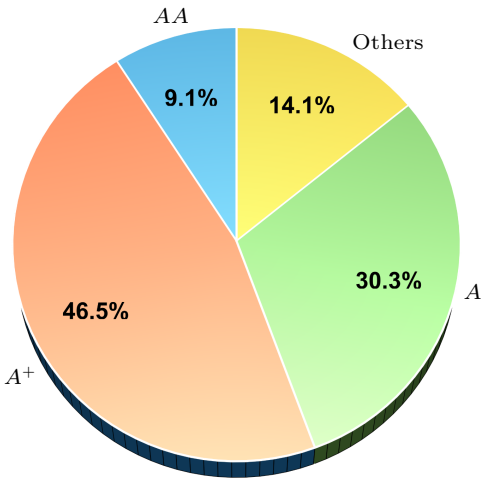


Fig. 4. Accuracy distribution of the calculated energy values for Al II.

3.2. Reduced transition matrix elements

We calculate the RMEs of relevant transitions using the CI + MBPT method. In the calculation of the reduced matrix elements, we have also taken the Breit interaction into account. The RMEs of E1, E2, M1, and M2 transitions arising from the five lowest energy states are presented in Tables S3–S6 of supplementary material (E1 in Table S3, E2 in Table S4, M1 in Table S5, and M2 in Table S6). The available theoretical and experimental values from Refs. [2,9,16,18–22,24,36,37,40] are also included for comparison. For the E1 RMEs, both the length gauge and velocity gauge are presented, as their agreement provides a valuable metric for assessing calculation uncertainties. Previous studies have established that the length gauge typically yields more accurate results for electric dipole transitions.[2,21] We are only concerned with the magnitude of the RMEs; thus, their absolute values are presented by default.

Our calculated RMEs show good agreement with existing theoretical and experimental values.[2,9,16,18–22,24,36,37,40] For stronger transitions, such as the $3s^2\ {}^1S_0$–$3s3p\ {}^1P_1$ transition, the differences between our results and other reference values are less than 10%, while for weaker transitions, the relative differences are less than 40%. For E1 transitions, most differences between the length gauge and velocity gauge are less than 1% for stronger transitions and 10% for weaker transitions. As far as we know,[2,9,16,18–22,24,36,37,40] many of our calculations present the first theoretical predictions for these transitions. The large magnitudes of these previously unreported RMEs, such as the $3s3p\ {}^3P_0$–$3s4p\ {}^3P_2$ (E2) transition, suggest significant transition strengths, warranting future experimental investigation. Specifically, our computational results demonstrate good agreement with the Papoulia *et al.*[14] dataset, with over 90% of comparative parameters showing discrepancies below 1%. However, for the oscillator strengths calculated from RMEs, our results are mostly closer to the NIST database values compared with the results of Ref. [14]. For example, the transitions $3s^2\ {}^1S_0$–$3s3p\ {}^3P_1$, $3s^2\ {}^1S_0$–$3s3p\ {}^1P_1$, $3s3p\ {}^1P_1$–$3s3d\ {}^1D_2$, etc.

3.3. Transition probabilities and oscillator strengths

Using Eqs. (6)–(13) and wavelengths from the NIST database, we calculate transition probabilities and oscillator strengths for the transitions presented in Tables S3–S6 of the supplementary material. Comparison with NIST reference data demonstrates excellent agreement, with most calculated values differing by less than 10% from the NIST values. For more than ten transitions, the agreement is particularly strong, with differences below 1%. Transitions that differ significantly from the data in the NIST-related databases are mostly weak transitions or involve relatively high upper states. Equations (6)–(13) reveal that, when only the variation of the reduced matrix elements is considered, the error in the transition probability is twice that in the reduced matrix elements. An interesting case emerges for transitions such as $3s^2\ {}^1S_0$-$3s3p\ {}^3P_1$ (E1) and $3s3p\ {}^3P_0$-$3s3p\ {}^3P_2$ (E2), where we observe substantial differences in reduced matrix elements compared with previous calculations; however, the resulting transition probabilities show remarkably small deviations from the NIST database values. This consistency in transition probabilities provides strong validation of our computational approach and offers valuable insights for uncertainty estimation in Al II precision measurements, particularly for quantum optical clock experiments. Furthermore, our work extends beyond existing NIST data by providing predictions for previously unreported transitions, including $3s3p\ {}^3P_0$-$3s3p\ {}^3P_1$ (M1), $3s^2\ {}^1S_0$-$3s3d\ {}^1D_2$ (E2), etc. These new results establish important theoretical benchmarks for future experimental and theoretical

investigations of Al II. The accuracy of transition probabilities is evaluated by comparing our theoretical transition data with NIST values and can be classified according to the NIST ASD terminology ($AA \leq 1\%$, $A+ \leq 2\%$, $A \leq 3\%$, $B+ \leq 7\%$, $B \leq 10\%$, $C+ \leq 18\%$, $C \leq 25\%$, $D+ \leq 40\%$, $D \leq 50\%$, and $E > 50\%$).[25] The accuracy distribution of data with NIST database references is shown in Fig. 5.

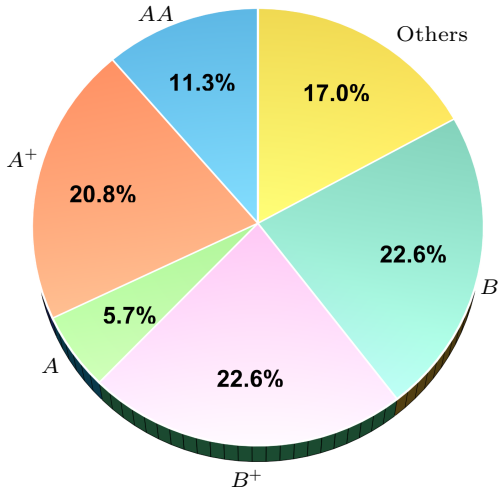


Fig. 5. Accuracy distribution of the transition probabilities for Al II.

4. Conclusion

We have conducted comprehensive relativistic calculations of atomic properties for the Al II ion using the configuration interaction plus many-body perturbation theory (CI + MBPT) method. We present accurate energy levels for the 103 lowest-lying states of Al II and comprehensive multipole transition data, including reduced matrix elements, transition probabilities, and oscillator strengths, for transitions originating from the five most important low-lying configurations ($3s^2$ $^1S_0$, $3s3p$ $^3P_0$, $3s3p$ $^3P_1$, $3s3p$ $^3P_2$, and $3s3p$ $^1P_1$) among these levels. Our calculated energy levels demonstrate excellent agreement with values from the NIST atomic spectra database, showing deviations below 0.2% for most states. The computed transition properties show good agreement with available theoretical and experimental values, with differences typically below 10% and achieving better than 1% agreement for strong transitions. Notably, our results predict transition properties for numerous previously unexplored transitions, substantially expanding the available atomic data for Al II. These high-accuracy predictions establish important benchmarks for future Al II precision measurements and astrophysical spectroscopy applications.

Data availability statement

The data that support the findings of this study are openly available in the supplementary material and in Science Data Bank at the following link: https://doi.org/10.57760/sciencedb.28555.

Acknowledgments

We would like to thank Prof. M. G. Kozlov of Petersburg Nuclear Physics Institute for the helpful assistance with the use of the CI + MBPT package. We also thank Dr. J. S. Liu for the helpful discussion. This project was supported by the Science and Technology Department of Hubei Province (Grant No. 2025AFA004), the Science and Technology Development Fund (FDCT), Macao SAR (Grant Nos. 0024/2024/RIB1, 0136/2024/RIA2, and 0004/2025/RDP), Shanghai Municipal Science and Technology Major Project (Grant No. 2019SHZDZX01), the Department of Science and Technology of Guangdong Province (Grant No. 2024QN11C352), and the National Natural Science Foundation of China (Grant No. 12404421).

References

[1] Rosenband T, Schmidt P O, Hume D B, Itano W M, Fortier T M, Stalnaker J E, Kim K, Diddams S A, Koelemeij J C J, Bergquist J C and Wineland D J 2007 *Phys. Rev. Lett.* **98** 220801
[2] Safronova M S, Kozlov M G and Clark C W 2011 *Phys. Rev. Lett.* **107** 143006
[3] Shang J J, Cui K F, Cao J, Wang S M, Chao S J, Shu H L and Huang X R 2016 *Chinese Phys. Lett.* **33** 103701
[4] Cui K F, Shang J J, Chao S J, Wang S M, Yuan J B, Zhang P, Cao J, Shu H L and Huang X R 2018 *J. Phys. B: At. Mol. Opt. Phys.* **51** 045502
[5] Keller J, Burgermeister T, Kalincev D, Didier A, Kulosa A P, Nordmann T, Kiethe J and Mehlstäubler T E 2019 *Phys. Rev. A* **99** 013405
[6] Brewer S M, Chen J S, Hankin A M, Clements E R, Chou C W, Wineland D J, Hume D B and Leibrandt D R 2019 *Phys. Rev. Lett.* **123** 033201
[7] Marshall M C, Castillo D A R, Arthur-Dworschack W J, Aeppli A, Kim K, Lee D, Warfield W, Hinrichs J, Nardelli N V, Fortier T M, Ye J, Leibrandt D R and Hume D B 2025 *Phys. Rev. Lett.* **135** 033201
[8] Chou C W, Hume D B, Koelemeij J C J, Wineland D J and Rosenband T 2010 *Phys. Rev. Lett.* **104** 070802
[9] Brewer S M, Chen J S, Beloy K, Hankin A M, Clements E R, Chou C W, McGrew W F, Zhang X, Fasano R J, Nicolodi D, Leopardi H, Fortier T M, Diddams S A, Ludlow A D, Wineland D J, Leibrandt D R and Hume D B 2019 *Phys. Rev. A* **100** 013409
[10] Cui K F, Chao S J, Sun C L, Wang S M, Zhang P, Wei Y F, Yuan J B, Cao J, Shu H L and Huang X R 2022 *Eur. Phys. J. D* **76** 140
[11] Ma Z Y, Deng K, Wang Z Y, Wei W Z, Hao P, Zhang H X, Pang L P, Wang B, Wu F F, Liu H L, Yuan W H, Chang J H, Zhang J X, Wu X Q, Zhang J and Lu Z H 2024 *Phys. Rev. Appl.* **21** 044017
[12] Wei Y F, Chao S J, Cui K F, Li C B, Yu S C, Zhang H, Shu H L, Cao J and Huang X R 2024 *Phys. Rev. Lett.* **133** 033001
[13] Cashman F H, Kulkarni V P, Kisielius R, Ferland G J and Bogdanovich P 2017 *Astrophys. J., Suppl. Ser.* **230** 8
[14] Papoulia A, Ekman J and Jönsson P 2019 *Astron. Astrophys.* **621** A16
[15] Li X F, Jiang G, Wang H B and Sun Q 2017 *Chin. Phys. B* **26** 013101
[16] Stanek M, Lowacki L G and Migdalek J 1996 *J. Phys. B: At. Mol. Opt. Phys.* **29** 2985
[17] Li W, Rynkun P, Radžiuť L, Gaigalas G, Atalay B, Papoulia A, Wang K, Hartman H, Ekman J, Brage T, Chen C Y and Jönsson P 2020 *Astron. Astrophys.* **639** A25
[18] Das B P and Idrees M 1990 *Phys. Rev. A* **42** 6900
[19] Mitroy J, Zhang J Y, Bromley M W J and Rollin K G 2009 *Eur. Phys. J. D* **53** 15
[20] Kallay M, Nataraj H S, Sahoo B K, Das B P and Visscher L 2011 *Phys. Rev. A* **83** 030503

[21] Kumar R, Chattopadhyay S, Angom D and Mani B K 2011 *Phys. Rev. A* **103** 022801
[22] Yu Y M, Suo B B and Fan H 2013 *Phys. Rev. A* **88** 052518
[23] Rosenband T, Hume D B, Schmidt P O, Chou C W, Brusch A, Lorini L, Oskay W H, Drullinger R E, Fortier T M, Stalnaker J E, Diddams S A, Swann W C, Newbury N R, Itano W M, Wineland D J and Bergquist J C 2008 *Science* **319** 1808
[24] Bohman M A, Porsev S G, Hume D B, Leibrandt D R and Safronova M S 2023 *Phys. Rev. A* **108** 053120
[25] Ralchenko Y, Kramida A E, Reader J and NIST ASD Team 2024 *NIST Atomic Spectra Database (Version 5.12)* Available: https://physics.nist.gov/asd. National Institute of Standards and Technology, Gaithersburg, MD.
[26] Dzuba V A, Flambaum V V and Kozlov M G 1996 *Phys. Rev. A* **54** 3948
[27] Kozlov M G, Porsev S G, Safronova M S and Tupitsyn I I 2015 *Comput. Phys. Commun.* **195** 199
[28] Yu Y M and Derevianko A 2018 *At. Data Nucl. Data Tables* **119** 263
[29] Tang Z M, Yu Y M, Jiang J and Dong C Z 2018 *J. Phys. B: At. Mol. Opt. Phys.* **51** 125002
[30] Lou Z S, Wang Y F, Kang B Y, Li R, Zhang W J, Wei Y F, Bu M L and Cai Y Y 2025 *Acta Phys. Sin.* **74** 103202
[31] Tang Z M, Wei Y F, Sahoo B K, Yang Y, Li C B, Zou Y M and Huang X R 2024 *Phys. Rev. A* **110** 043108
[32] Wei Y F, Tang Z M, Li C B, Yang Y, Zou Y M, Cui K F and Huang X R 2022 *Chin. Phys. B* **31** 083102
[33] Wei Y F, Tang Z M, Li C B and Huang X R 2024 *Acta Phys. Sin.* **73** 103103
[34] Wu L, Wang X, Wang T, Jiang J and Dong C Z 2023 *New J. Phys.* **25** 043011
[35] Li F C, Qiao H X, Tang Y B and Shi T Y 2022 *J. Quant. Spectrosc. Radiat. Transf.* **288** 108241
[36] Safronova U I and Safronova A S 2014 *Phys. Rev. A* **90** 012519
[37] Johnson W R, Safronova M S and Safronova U I 1997 *Phys. Scr.* **56** 252
[38] Morton D C 1991 *Astrophys. J. Suppl. Ser.* **77** 119
[39] Santana J A 2016 *At. Data Nucl. Data Tables* **111** 87
[40] Ray D, Mukherjee P K and Roy H P 1986 *Astrophys. J.* **346** 1045